11th International Symposium on Turbulence and Shear Flow Phenomena (TSFP11)
Southampton, UK, July 30 to August 2, 2019

PHYSICAL MECHANISM OF DISSIMILAR HEAT TRANSFER ENHANCEMENT BY VORTEX TUBE IN PLANE COUETTE FLOW

Akira Kubo
Graduate School of Engineering Science
Osaka University
1–3 Machikaneyama, Toyonaka
Osaka 560-8351 Japan
kubo@tes.me.es.osaka-u.ac.jp

Genta Kawahara
Graduate School of Engineering Science
Osaka University
1–3 Machikaneyama, Toyonaka
Osaka 560-8351 Japan
kawahara@me.es.osaka-u.ac.jp

Masaki Shimizu
Graduate School of Engineering Science
Osaka University
1–3 Machikaneyama, Toyonaka
Osaka 560-8351 Japan
shimizu@me.es.osaka-u.ac.jp

ABSTRACT

From the viewpoint of efficient energy use, it is necessary to implement the flow enhancing heat transfer while suppressing flow resistance by momentum transfer. However, it is generally difficult to realize dissimilar heat transfer enhancement, i.e., more heat transfer and less momentum transfer, owing to strong similarity between heat and momentum transfer. Recent studies have suggested that the vortex which has the same sign of vorticity as that of the background shear flow (the cyclonic vortex) is effective in dissimilar heat transfer enhancement. But, it has not yet been known why the cyclonic vortex achieves dissimilar heat transfer, or if another type of vortices would also lead to dissimilarity. In order to tackle these problems, we introduce directly a vortex tube into laminar plane Couette flow under various conditions and investigate heat and momentum transfer by these vortices. As a consequence, the physical mechanism of dissimilarity emergence has been elucidated by interpreting the distribution of streamwise pressure gradient and the resulting difference between temperature and velocity in terms of an exact solution to the Euler equation and the Lagrangian observation of the streamwise pressure gradient and the resulting temperature-velocity difference, respectively.

1 INTRODUCTION

Heat exchangers are widely used for engineering applications, such as personal computers, air conditioners, automobiles, etc. Hence it is definitely beneficial for us to improve the performance of heat exchangers. In order to achieve that, it suffices to realize heat transfer enhancement which is superior to the flow resistance by momentum transfer. However, it is generally difficult to realize dissimilar heat transfer enhancement, i.e., more heat transfer and less momentum transfer, owing to strong similarity between heat and momentum transfer (Reynolds (1874); Chilton & Colburn (1934)), i.e., if one is increased, the other is also increased. This similarity stems from the existence of the similar terms in the governing equations of the streamwise velocity and temperature. Nevertheless, since there is a difference in the pressure term between these two governing equations, weak dissimilarity is inherent even if the ratio of the kinematic viscosity coefficient and the thermal diffusion coefficient (the Prandtl number) is unity. Hence, we can say that although it is difficult to realize dissimilar heat transfer enhancement, it might be possible as a consequence of ingenious contrivance.

In several prior studies, attempts were made to achieve dissimilar heat transfer enhancement. By experimentally examining the variation of heat and momentum transfer caused by installing a rectangular lib in the channel flow, Suzuki *et al.* (1991) showed that the vortex with the same sign of the spanwise vorticity as the background shear flow (the cyclonic vortex) is effective in dissimilar heat transfer enhancement. Katoh *et al.* (2012) investigated the tubular vortices in turbulent channel flow, and found that they often incline from the streamwise direction in the spanwise direction so that their spanwise vorticity may exhibit the same sign as the mean shear, i.e. cyclonic vortices, and subsequently they contribute to dissimilarity. The existence of the cyclonic vortices was also confirmed in the flow field realizing large dissimilarity by implementing blowing and suction on the walls in channel flow (Yamamoto *et al.* (2013); Kasagi *et al.* (2012)). More recently, by using a variational method Motoki *et al.* (2018) reported that numerous tilted vortices which have the opposite sign of vorticity to the background shear flow, i.e. anti-cyclonic vortices, exist in the incompressible flow field maximizing heat transfer although the obtained field does not satisfy the Navier–Stokes equation.

From the previous studies mentioned above, the cyclonic vortices may be beneficial for dissimilar heat transfer enhancement; however, the following questions arise. Why

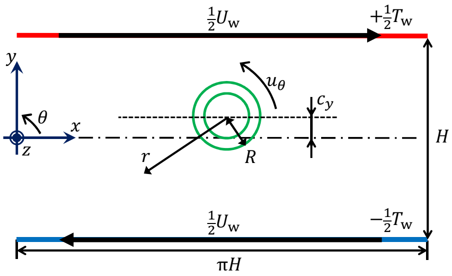

Figure 1. Flow configuration. The green circles denote the streamlines of the introduced vortex.

can the cyclonic vortex achieve dissimilar heat transfer enhancement? Can the anti-cyclonic vortex also lead to dissimilarity? If so, why?

In this study, therefore, we try to elucidate the physical mechanism of dissimilarity emergence. In order to achieve this purpose, numerical simulation of the transfer process of heat and momentum is carried out for the flow field in which a vortex tube is introduced under various conditions, and the influence of the vortex on heat and momentum transfer is investigated.

Since we pay attention only to dissimilarity due to vortices, the boundary conditions of the streamwise velocity and temperature are consistent and the Prandtl number is set to unity. In order to simplify the dissimilarity mechanism to be discussed, we suppose that the single vortex is straight and uniform in its axial direction so as not to consider the self- or mutual-interaction of the vortices. For the same reason, the Reynolds number is assumed to be in the range of laminar flow where any vortices will not appear autonomously.

2 FORMULATION

2.1 Flow configuration and governing equations

We consider heat and momentum transfer enhancement by the introduction of a straight vortex tube in plane Couette flow and an associated thermal conduction state, which is one of the simplest configurations in the sense that internal heat source (corresponding to mean pressure gradient) is not necessary for consistency of momentum and heat transfer. Figure 1 shows the flow configuration. The flow is driven by two parallel plates of distance H, moving in the opposite directions at a constant speed $U_w/2$. The upper (or lower) wall surface is kept at higher (or lower) constant temperature $+T_w/2$ (or $-T_w/2$). The coordinates x, y and z are taken in the streamwise, the wall-normal and the spanwise directions, respectively. The upper (or lower) wall is located at $y = +H/2$ (or $y = -H/2$). A periodic boundary condition is imposed on the x-direction and its period is taken as πH.

The working fluid is Newtonian, and the components of velocity $\boldsymbol{u}$ in the streamwise, the wall-normal and the spanwise directions are u, v and w, respectively. The temperature T is assumed to be a passive scalar and follows the advection-diffusion equation, because we target situations where the Eckert number is small enough.

The nondimensionalized governing equations of the velocity and temperature, and the nondimensionalized boundary conditions by the wall separation H, the wall speed difference U_w and the wall temperature difference T_w can be written as

$$\nabla^* \cdot \boldsymbol{u}^* = 0, \tag{1}$$

$$\frac{\partial \boldsymbol{u}^*}{\partial t^*} + \boldsymbol{u}^* \cdot \nabla^* \boldsymbol{u}^* = -\nabla^* p^* + \frac{1}{Re}\Delta^* \boldsymbol{u}^*, \tag{2}$$

$$\frac{\partial T^*}{\partial t^*} + \boldsymbol{u}^* \cdot \nabla^* T^* = \frac{1}{RePr}\Delta^* T^*, \tag{3}$$

$$\boldsymbol{u}^*\left(y^* = \pm\frac{1}{2}\right) = \left(\pm\frac{1}{2}, 0, 0\right), \tag{4}$$

$$T^*\left(y^* = \pm\frac{1}{2}\right) = \pm\frac{1}{2}, \tag{5}$$

$$[u^*, v^*, w^*](x^*, y^*) = [u^*, v^*, w^*](x^* + \pi, y^*), \tag{6}$$

$$T^*(x^*, y^*) = T^*(x^* + \pi, y^*), \tag{7}$$

where t is the time and p is the pressure, and the superscript * means the dimensionless physical quantity. The Reynolds number is defined as $Re = U_w H/\nu$, and the Prandtl number $Pr = \nu/\alpha$ is set to unity, where ρ is the mass density of the fluid, ν is the kinematic viscosity coefficient and α is the thermal diffusion coefficient. Hereafter, the superscript * is dropped, and all the physical quantities are described as dimensionless quantities unless otherwise noted.

We introduce single axially uniform vortex into Couette flow so as not to consider the self- or mutual-interaction of the vortices. Using the toroidal/poloidal decomposition, the circumferential velocity of the vortex to be introduced at $t = 0$ is given by

$$u_\theta = A\frac{r}{R^2}\exp\left(-\frac{r^2}{2R^2}\right) \times [\text{filter}], \tag{8}$$

$$[\text{filter}] = \begin{cases} 1 - \text{sech}^{500}\left(y - \frac{1}{2}\right) & \left(0 < y \le +\frac{1}{2}\right) \\ 1 - \text{sech}^{500}\left(y + \frac{1}{2}\right) & \left(-\frac{1}{2} \le y \le 0\right). \end{cases} \tag{9}$$

In order to satisfy the wall boundary condition (4), the filter (9) is applied. A is the amplitude of the circumferential velocity, and R is the vortex radius. The center of the vortex is located at $(x, y) = (c_x, c_y)$. r is the distance from the vortex axis, i.e. $r^2 = (x - c_x)^2 + (y - c_y)^2$.

We define the cyclonic (or anti-cyclonic) vortex as a vortex which has same (or opposite) sign of vorticity as that of the background shear flow. In Figure 1, the rotation direction of the cyclonic (or anti-cyclonic) vortex is clockwise ($u_\theta < 0$) (or counterclockwise ($u_\theta > 0$)).

2.2 Dissimilarity indicator

As an indicator of dissimilarity,

$$D = (St - c_f)Re \tag{10}$$

is used.

The wall-average Stanton number and the friction coefficient are defined, respectively, by

$$St = \frac{1}{2RePr}\left\langle \left.\frac{\partial T}{\partial y}\right|_{y=-1/2} + \left.\frac{\partial T}{\partial y}\right|_{y=+1/2} \right\rangle_x, \tag{11}$$

$$c_f = \frac{1}{2Re}\left\langle \left.\frac{\partial U}{\partial y}\right|_{y=-1/2} + \left.\frac{\partial U}{\partial y}\right|_{y=+1/2} \right\rangle_x, \tag{12}$$

Table 1. Parameter values in numerical simulations.

Re	200, 400, 600
A	±0.05, ±0.1, ±0.2
R	0.025, 0.05, 0.1
c_y	0, 0.15 0.3

where

$$\langle\!\langle \,\cdot\, \rangle\!\rangle_x = \frac{1}{\pi}\int_0^{\pi} (\,\cdot\,)\,\mathrm{d}x. \tag{13}$$

They represent the dimensionless intensity of heat transfer and momentum transfer, respectively. Note that they take a value of Re in laminar flow (without the introduced vortex).

In the case of $D > 0$, heat transfer is larger than momentum transfer, implying dissimilar heat transfer enhancement. Dissimilar heat transfer enhancement in this paper leads to good dissimilarity in an engineering sense. On the other hand, in the case of $D < 0$, heat transfer is smaller than momentum transfer, leading to bad dissimilarity. Hereafter, 'dissimilarity' simply implies the good dissimilarity.

2.3 Numerical method

Eqs. (1)-(7) are solved by direct numerical simulations (DNS), using the second-order central finite-difference method in space and the Huen method in time. The pressure p and the flow velocity $\boldsymbol{u}$ are coupled by the Maker And Cell (MAC) method. The uniform staggered grids are employed with the number of grid points being 256×257 in the x- and y-directions. It has been confirmed that even if the number of the gird points is doubled (512×513), the simulation results are consistent with the ones shown later.

The initial velocity field at $t=0$ is given by the introduction of the vortex (9) in laminar plane Couette flow ($\boldsymbol{u} = y\boldsymbol{e}_x + u_\theta\boldsymbol{e}_\theta$), while the initial temperature field at $t=0$ is in a thermal conductive state ($T=y$), where $\boldsymbol{e}_x$ and $\boldsymbol{e}_\theta$ are unit vectors in the streamwise and circumferential direction, respectively (see Figure 1). The parameters of this system are the Reynolds number Re, the amplitude of the circumferential velocity A, the position c_y and the radius R of the vortex. The values of the four flow parameters are chosen as shown in Table 1. Note that Reynolds number is assumed to be in the range of laminar flow. Positive (or negative) A means the circumferential velocity of the anti-cyclonic (or cyclonic) case. DNS is performed for the vortex introduction, starting from the initial conditions, to compute subsequent momentum and heat transfer until when the difference between the total kinetic energy $E = \frac{1}{2\pi}\iint\left(u^2+v^2+w^2\right)\mathrm{d}x\mathrm{d}y$ and that in laminar Couette flow without the introduced vortex $\frac{1}{2}$ is not greater than 10^{-9}.

3 DISSIMILARITY EMERGENCE

We will confirm whether cyclonic and anti-cyclonic vortices achieve more significant dissimilar heat transfer enhancement. In Figure 2, $\overline{D}$ of the cyclonic or anti-cyclonic vortex is shown as a function of the vortex Reynolds number $Re_\Gamma = \omega_{z,\max}R^2Re/2 = ARe$, where $\overline{(\cdot)}$ represents the time average over $t = 0$–t_{end}. Note that the vortex Reynolds

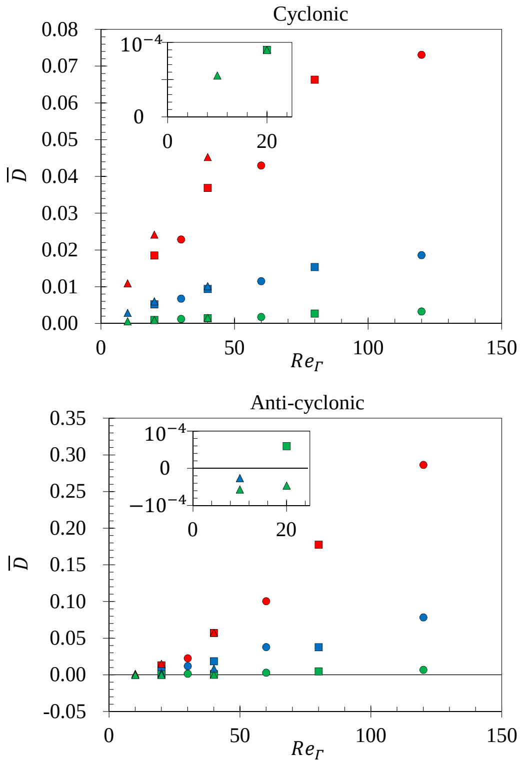

Figure 2. Dependence on the vortex Reynolds number of dissimilarity in the cyclonic (upper) and anti-cyclonic (lower) cases for the parameter values shown in Table 1 $c_y =$ 0. Triangle, square and circle symbols represent $Re = 200$, 400 and 600, respectively. Green, blue and red symbols represent $R = 0.025$, 0.05 and 0.1, respectively. The inset denotes the magnification of the small vortex Reynolds number range $0 \le Re_\Gamma \le 25$.

number is often used as dimensionless strength of the vortex. $\omega_{z,\max} = 2A/R^2$ is the maximum value of the component of the vorticity at the initial time $t=0$.

Although there are some exceptions when the vortex Reynolds number Re_Γ is small, i.e., the vortex is weak in the anti-cyclonic case (see §5), the vortex almost tends to realize dissimilarity.

Figure 2 is shown only for $c_y = 0$, but the same tendency has been observed even if $c_y = 0.15$ or 0.3.

4 PHYSICAL MECHANISM OF DISSIMILARITY EMERGENCE

As was mentioned in §3, the DNS data are inspected for the 'long-term' averaged from the initial time $t=0$ to the eventual time t_{end}, at which the introduced vortex is sufficiently attenuated. Hence any short-term events, e.g., emergence of transient structures in the instantaneous velocity and temperature fields stemming from the introduction of the vortex, must disappear from the averaged fields. Here, we shall discuss the 'universal' factors that contribute to the dissimilarity appearing in the long-term averaged field.

4.1 Pressure gradient

The trigger of dissimilarity should be the streamwise pressure gradient $\partial p/\partial x$, as mentioned in §1. The distribution of $\overline{\partial p/\partial x}$ obtained from the DNS data is shown in

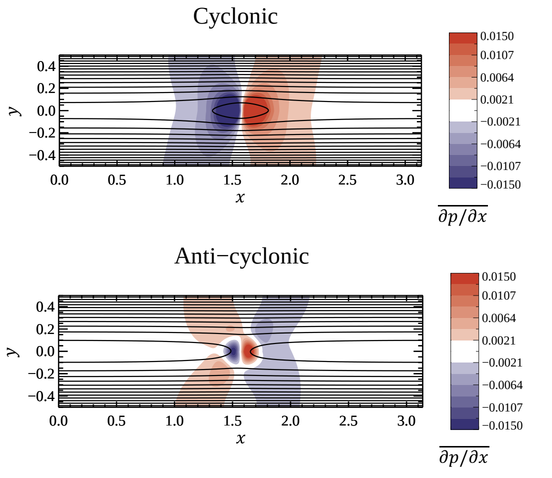

Figure 3. Spatial distribution of the time-averaged streamwise pressure gradient for $Re = 400, |A| = 0.2, R = 0.1, c_y = 0$. The black curves are the time-averaged streamlines. The cases of the cyclonic (anti-cyclonic) vortex are in the upper (lower) panel.

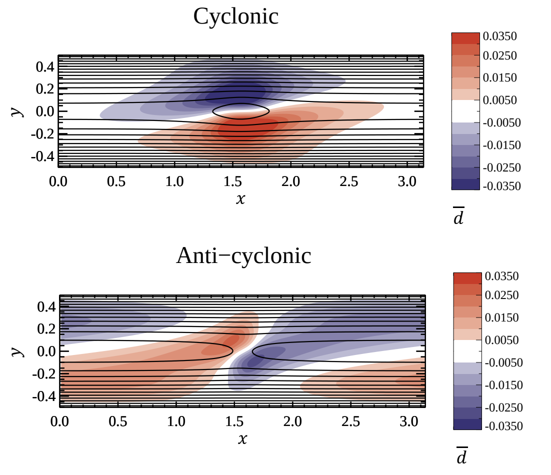

Figure 4. Spatial distribution of the time-averaged difference between the temperature and the streamwise velocity for $Re = 400, |A| = 0.2, R = 0.1, c_y = 0$. The black curves are the time-averaged streamlines. The cases of the cyclonic (anti-cyclonic) vortex is in the upper (lower) panel.

Figure 3. The pressure field of the cyclonic vortex (upper) is distributed such that the pressure decreases toward the vortex center near the vortex. On the other hand, that of the anti-cyclonic vortex (lower) is distributed such that the pressure decreases toward the center near the vortex but increases toward the center in the far region of the vortex. There is a significant difference in the streamwise pressure gradient between the cyclonic and anti-cyclonic cases expect for the central region of the vortices.

Here, we try to interpret theoretically the distribution of $\overline{\partial p/\partial x}$ around the cyclonic or the anti-cyclonic vortex (Figure 3). Since it is difficult to target the pressure gradient of the unsteady viscous flow field introduced with vortex, a steady inviscid two-dimensional flow field as shown below is considered: The vortex tube that has the circumferential velocity A/r, that is vortex filament, is introduced into a constant shear flow ($u = y$) in an infinite region with no boundary. A is the amplitude of the circumferential velocity, which means the cyclonic (or anti-cyclonic) vortex when it is negative (or positive).

The pressure field in this simple system was determined by Imai (1984) using complex potential theory. In this inviscid flow the pressure is rigorously given by

$$p = -\frac{1}{2}\frac{A^2}{r^2} + A\frac{y^2}{r^2} - A\ln r. \tag{14}$$

and thus the streamwise pressure gradient is

$$\frac{\partial p}{\partial x} = \left(\frac{A^2 - 2Ay^2}{r^4} - \frac{A}{r^2}\right)x. \tag{15}$$

If r is smaller, the first term of Eq. (15) $(A^2 - 2Ay^2)x/r^4$ is the more dominant. Hence regardless of the cyclonic and anti-cyclonic case, in the central region of the vortex, it can be considered that $\partial p/\partial x < 0$ on the left side ($x < 0$) and $\partial p/\partial x > 0$ on the right side ($x > 0$) in Figure 3. On the other hand, if r is larger, the second term $-Ax/r^2$ is the more dominant. Therefore, in the cyclonic (or anti-cyclonic) vortex, $\partial p/\partial x$ can be considered to take a negative (or positive) value on the left side ($x < 0$) (or the right side ($x > 0$)). It should be noted that the significant difference observed in the far region of the vortices is not dependent of the detailed vortex structure.

4.2 Difference between the temperature and the streamwise velocity

This pressure gradient leads to distinct distribution of the temperature and the streamwise velocity, and so we next see the distribution of their difference $d = T - u$ (Figure 4). Larger and smaller values of $\overline{d}$ are observed in the upper and lower regions of the cyclonic vortex (upper), while those are observed in the right and left regions of the anti-cyclonic vortex (lower).

Next, we also try to interpret the distribution of their difference $\overline{d}$. The governing equation of d is obtained from the difference of the x-component of Eq. (2) from Eq. (3), as

$$\frac{\mathrm{D}d}{\mathrm{D}t} = \frac{\partial p}{\partial x} + \frac{1}{Re}\Delta d. \tag{16}$$

From Eq. (16), it can be seen that d is related to $\partial p/\partial x$ via the Lagrangian time derivative. The trajectory of fluid particles, that is the streakline, passes through the central region of the cyclonic vortex, while it does not pass through that of the anti-cyclonic vortex (cf. Figure 3).

Following the motion of the fluid particle along the upper streaklines in the cyclonic case, we can see the change of d (Figure 5 left). Since $\partial p/\partial x$ is not significant in the left most region of the vortex, d would be almost null in the region I. When the fluid particle reaches the region II of $\partial p/\partial x < 0$, d gradually decreases to be negative. When it reaches the region III of $\partial p/\partial x > 0$, d increases to eventually return to zero in the region I$'$.

In the above consideration, only the influence of the first term on the right-hand side of Eq. (16) is taken into account. Now we consider the second term as well. Since Δd represents the diffusion of d, its effect can be interpreted

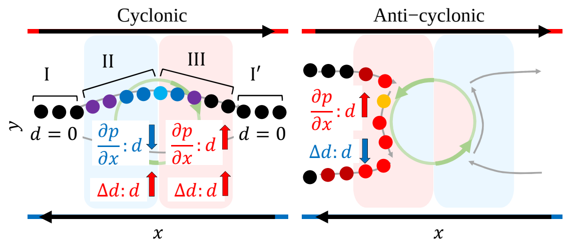

Figure 5. The upper (or left) trajectory of fluid particles (circular symbols) is shown in the cyclonic (or anti-cyclonic) vortex in the left (or right) panel. The color of the fluid particles represents the value of d, which decreases from zero to a negative value in order of black, violet, blue, light blue and increases from zero to a positive value in order of black, brown, red, yellow. The green and black arrows represent the streamlines of the vortex and the streaklines of the total flow, respectively. Red (or blue) area is positive (or negative) streamwise pressure gradient area.

as the 'resilience' about $d=0$. Therefore, Δd in the region II should interfere with the reduction of d by $\partial p/\partial x<0$. In other words, Δd has counter action against $\partial p/\partial x<0$. Note that it is not the case in the region III where $\partial p/\partial x>0$ while still $d<0$. As a result, the rate of change in d is more significant downstream of the vortex (the region III) than upstream (the region II), implying that d can be restored faster to zero downstream of the vortex. It turns out that in the upper (or lower) part of the cyclonic vortex the region of $d<0$ (or $d>0$) should be slightly biased upstream, as shown in Figure 4 (upper).

Much simpler argument suggests that in the anti-cyclonic case (Figure 5 right), the region of $d>0$ (or $d<0$) appears on the left (or right) of the vortex where $\partial p/\partial x>0$ (or $\partial p/\partial x<0$), as shown in Figure 4 (lower).

4.3 Difference between the turbulent heat flux and the Reynolds stress

Dissimilar heat transfer enhancement can be quantified as $D=(St-c_f)Re$. Mutiplying Eq. (16) by the wall-normal coordinate y and then integrating the product over the whole domain, D is given by

$$D=\frac{Re}{2}\left(\left\langle y\frac{\partial d}{\partial t}\right\rangle_{xy}-\langle dv\rangle_{xy}\right), \tag{17}$$

where

$$\langle(\ \cdot\ )\rangle_{xy}=\frac{1}{\pi}\int_0^{\pi}\int_{-\frac{1}{2}}^{+\frac{1}{2}}(\ \cdot\ )\,\mathrm{d}x\mathrm{d}y. \tag{18}$$

If we consider the 'long-term' average $\overline{D}$, the contribution from the first integrand $\langle y\partial d/\partial t\rangle_{xy}$ in Eq. (17) can be neglected (see §5), suggesting that the dissimilarity $\overline{D}$ can be expressed by the volume integral of the difference between the turbulent heat flux $-\overline{Tv}$ and the Reynolds stress $-\overline{uv}$, that is $-\overline{dv}$. The distribution of $-\overline{dv}$ obtained from the DNS data is shown in Figure 6. It follows from this figure that the region of $-\overline{dv}>0$ is much larger than that of $-\overline{dv}<0$ in both the cyclonic and the anti-cyclonic cases, leading to dissimilarity.

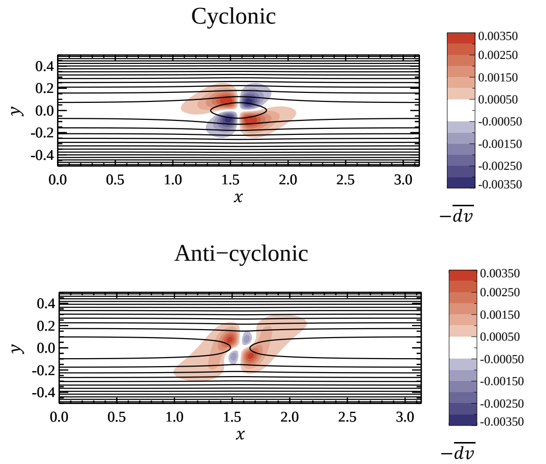

Figure 6. Spatial distribution of the time-averaged difference between the turbulent heat flux and the Reynolds stress for $Re=400, |A|=0.2, R=0.1, c_y=0$. The black curves are the time-averaged streamlines. The cases of the cyclonic (anti-cyclonic) vortex are in the upper (lower) panel.

Let us now interpret the distribution of $-\overline{dv}$. Since the wall-normal velocity v is induced by the vortex and the distribution of d is described as in Figure 4, $-\overline{dv}$ can be infered as in Figure 6.

For the sake of simplicity of interpretation, this study has been targeted to a laminar flow field. However, it has been numerically confirmed that the proposed physical mechanism also holds for the cyclonic or anti-cyclonic vortex introduced in turbulent plane Couette flow if the introduced vortex dominates over the nearby vortices.

5 REMARKS ON THE WEAK ANTI-CYCLNIC VORTEX

In this section, we interpret why the weak anti-cyclonic vortices lead to bad dissimilarity in Figure 2. To go straight to the point, due to the short decay time of the weak vortex, the DNS data are 'not' inspected for the long-term averaged over $t=0$–t_{end}, in other words $\langle y\partial d/\partial t\rangle_{xy}$ in Eq. (17) cannot be neglected.

The Re_Γ-dependency on the magnitude relationship between $\overline{\langle y\partial d/\partial t\rangle}_{xy}$ and $-\overline{\langle dv\rangle}_{xy}$ is shown in Figure 7.

From Figure 7, although the contribution of $\overline{\langle y\partial d/\partial t\rangle}_{xy}$ to dissimilarity is several times larger than that of $-\overline{\langle dv\rangle}_{xy}$ in the weaker-vortex case of smaller Re_Γ, its magnitude relation reverses as the vortex becomes stronger. In the case of the strong vortex, $-\overline{\langle dv\rangle}_{xy}$ is several times to ten times larger than that of $\overline{\langle y\partial d/\partial t\rangle}_{xy}$. It is considered that the time required for the attenuation of the vortex is related to these results.

Next, let us now consider $\overline{\langle y\partial d/\partial t\rangle}_{xy}$. There is no difference between the temperature and streamwise velocity at time t_{end}, and so $\overline{\langle y\partial d/\partial t\rangle}_{xy}$ can be approximated as

$$\overline{\left\langle y\frac{\partial d}{\partial t}\right\rangle}_{xy}\approx-\left\langle y\frac{d_0}{t_{\mathrm{end}}}\right\rangle_{xy} \tag{19}$$

by using the initial condition, $d_0=T_0-u_0$, where T_0 and u_0 are the temperature and streamwise velocity at the initial time, respectively.

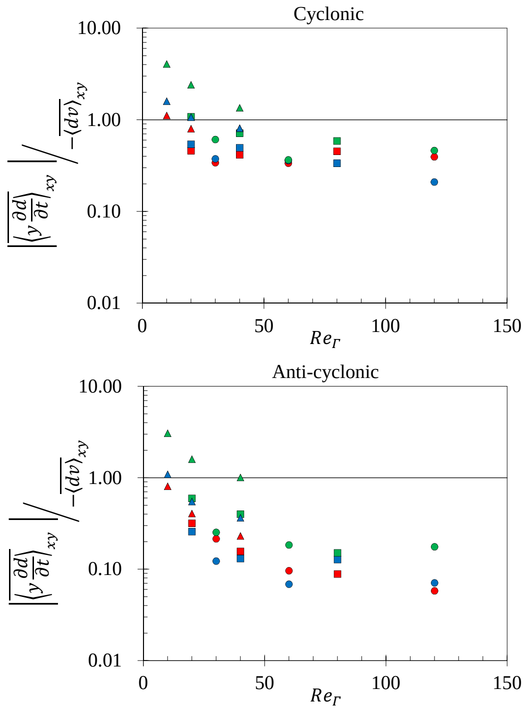

Figure 7. Dependence on the vortex Reynolds number of $\overline{\langle y\partial d/\partial t\rangle_{xy}}$ and $-\overline{\langle dv\rangle_{xy}}$ in the cyclonic (left) and the anti-cyclonic (right) cases for the parameter values shown in Table 1 $c_y = 0$. Triangle, square and circle symbols represent $Re = 200$, 400 and 600, respectively. Green, blue and red symbols represent $R = 0.025$, 0.05 and 0.1, respectively.

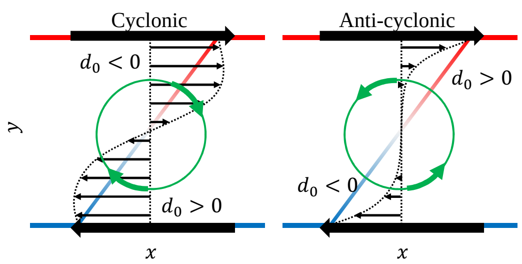

Figure 8. Conceptual diagram of difference between the temperature field and the streamwise velocity field at initial conditions in the cyclonic (left) and the anti-cyclonic (right) cases.

Since the cyclonic vortex accelerates the streamwise velocity, $|u_0| > |T_0|$, leading to $-\langle yd_0/t_{\mathrm{end}}\rangle_{xy} > 0$. On the other hand, since the anti-cyclonic vortex decelerates it, $|u_0| < |T_0|$, leading to $-\langle yd_0/t_{\mathrm{end}}\rangle_{xy} < 0$ (see Figure 8).

Therefore, owing to the contribution from $\overline{\langle y\partial d/\partial t\rangle_{xy}}$, which exerts a bad effect on the anti-cyclonic vortex in the sense of dissimilar heat transfer enhancement, the anti-cyclonic vortex realizes bad dissimilarity, when the vortex is weak.

It should be noted that $\overline{\langle y\partial d/\partial t\rangle_{xy}}$ is not related to the nature of the vortex but to initial or terminal condition. Hence $\overline{\langle y\partial d/\partial t\rangle_{xy}}$ is not essential for 'universal' dissimilarity.

REFERENCES

Chilton, T. H. & Colburn, A. P. 1934 Mass transfer (absorption) coefficients prediction from data on heat transfer and fluid friction. *Journal of Fluid Mechanics* **26**, 1183–1187.

Imai, I. 1984 Unsteady motion of fluid. *RIMS Kokyuroku* **510**, 1–17.

Kasagi, N., Hasegawa, Y., Fukagata, K. & Iwamoto, K. 2012 Control of turbulent transfer less friction and more heat transfer. *ASME Journal of Heat Transfer* **134**, 031009.

Katoh, K., Sakai, A., Fujii, R., Wakimoto, T. & Kawahara, G. 2013 Influence of spanwise vorticity on dissimilarity between turbulent momentum and heat transfer. *Trans. JSME B.* **79**, 2019–2029.

Katoh, K., Wakimoto, T. & Nishioka, N. 2012 The influence of pressure gradient-wall normal velocity correlation on turbulent prandtl number. *Trans. JSME B.* **78**, 1784–1797.

Motoki, S., Kawahara, G. & Shimizu, M. 2018 Optimal heat transfer enhancement in plane couette flow. *Journal of Fluid Mechanics* **835**, 1157–1198.

Reynolds, O 1874 On the extent and action of the heating surface of the steam boilers. *Manchester Prodeedings of the Literary Philosophical Society* **14**, 7–12.

Suzuki, H., Suzuki, K., Inoue, Y. & Hagiwara, Y. 1991 Unsteady flow and heat transfer in a channel obstructed by a square rod (3rd report, characteristics and mechanism of heat transfer). *Trans. JSME B.* **57**, 1403–1409.

Yamamoto, A., Hasegawa, Y. & Kasagi, N. 2013 Optimal control of dissimilar heat and momentum transfer in a fully developed turbulent channel flow. *Journal of Fluid Mechanics* **733**, 189–220.